Available online at www.sciencedirect.com
SCIENCE DIRECT®
Journal of Power Sources 134 (2004) 153–159
JOURNAL OF POWER SOURCES
www.elsevier.com/locate/jpowsour

Proton conductivity in stoichiometric and sub-stoichiometric yttrium doped $SrCeO_3$ ceramic electrolytes

N. Sammes [a], R. Phillips [b], A. Smirnova [a,*]

[a] *Connecticut Global Fuel Cell Center, University of Connecticut, 44 Weaver Road, Unit 5233, Storrs, CT 06269, USA*
[b] *Department of Materials and Process Engineering, University of Waikato, Private Bag 3105, Hamilton, New Zealand*

Received 27 January 2004; accepted 14 February 2004

Available online 2 July 2004

Abstract

The crystal structure and electrical properties of stoichiometric perovskite proton conductors $SrCe_{1-x}Y_xO_{3-\delta}$ (where $x = 0.025$, 0.05, 0.075, 0.1, 0.15, and 0.2 and $\delta = x/2$) and substoichiometric $Sr_{0.995}Ce_{0.95}Y_{0.05}O_{3-\delta}$ have been investigated. The conductivities of the samples were measured as a function of the partial pressure of oxygen at 600 and 800 °C, and at two water vapor pressures ($P_{H_2O} = 0.01$ and 0.001 atm). A P_{O_2} range of 1 atm (pure O_2) to approximately 1×10^{-25} atm (N_2/H_2 mix) allowed for the separation of n-(electron), p-(hole), and i-(ionic) type conductivities.

In the case of stoichiometric perovskite proton conductors, the unit cell volume (UCV) and calculated density decrease with increasing yttrium content. The ionic and p-type components of the conductivity show threshold effect with Y-doping, which may be related to the double substitution of Y on both A- and B-sites. A maximum ionic conductivity of 5 mS/cm is found at 10% Y, whereas p-type conductivity increases with increasing yttrium concentration. A conductivity component appearing at low oxygen partial pressures decreases with yttrium doping. The substoichiometric material showed a drop in unit cell volume of approximately 0.34 Å^3 compared to its stoichiometric partner. The conductivity components of substoichiometric material are higher than the conductivities of corresponding stoichiometric material, being approximately 7 mS/cm for both P_{H_2O} levels.

Keywords: Ceramics; X-ray diffraction; Perovskites; Protonic conductors; Electrical conductivity; Substoichiometric materials

1. Introduction

Mixed conducting protonic ceramic materials are of considerable interest for applications in hydrogen sensors, electrocatalytic reactors for hydrogen separation, steam electrolyzes, and as electrolytes in intermediate temperature fuel cells operating on hydrocarbon fuels [1].

The systematic investigation of proton conducting perovskite type oxides started with the work of Takahashi and Iwahara in 1980 [2]. Several oxides have been shown to be good conductors, the most well known of these are the acceptor doped Sr and Ba cerates, and Sr, Ba, and Zr zirconates. These oxides have been investigated for possible use in SOFC, hydrogen separation membranes, and hydrogen sensors [3–7].

A typical example of a proton conducting oxide of this class is the substituted solid solution material based on the perovskite oxide $SrCeO_3$, $SrCe_{0.95}Yb_{0.05}O_{2.975}$, which exhibits protonic conduction in water and hydrogen containing atmospheres at elevated temperatures [3].

This material is a substituted solid solution based on the perovskite-type oxide $SrCeO_3$, in which Yb replaces 5% of Ce. Other perovskite-type oxides based on $SrCeO_3$ and $BaCeC_3$, in which tnvalent cations are partially substituted for cerium, are also protonic conductors under the same conditions described above [8,9]. The general formula is written as $SrCe_{1-x}M_xO_{3-\delta}$ or $BaCe_{1-x}M_xO_{3-\delta}$, where M is a rare earth element, x is less than its upper limit of solid solution formation range (usually less than 0.2), and δ is the oxygen deficiency per unit formula, normally $x/2$. Their protonic conductivities in hydrogen atmosphere are of the order of 10^{-3} to 10^{-2} S/cm at 600–1000 °C [10].

After the discovery of $SrCeO_3$ based protonic conductors, $KTaO_3$-based oxides [11] were reported to have protonic conduction at high temperatures (3.5×10^{-3} S/cm), although the conductivities were not as high as those of the cerate-based perovskite type oxide ceramics. Some doped zirconates based on $CaZrO_3$, $SrZrO_3$, or $BaZrO_3$ [12] were

* Corresponding author. Tel.: +1-860-486-8762; fax: +1-860-486-8378.
E-mail address: alevtina@angr.uconn.edu (A. Smirnova).

0378-7753/$ – see front matter © 2004 Elsevier B.V. All rights reserved.
doi:10.1016/j.jpowsour.2004.02.036

also confirmed to exhibit the same behavior as the cerates although their conductivities were rather low.

Among the oxides described above, $BaCeO_3$-based ceramics show the highest conductivity, approximately, 5.5 $\times$ 10^{-1} S/cm at 1000 °C for $BaCe_{0.9}Nd_{0.1}0_{3-\delta}$ [10]. However, the contribution of oxygen ions to the total conduction increases markedly as the temperature is raised [13–15]. At 100 °C, although the conductivity of BaCeCV based ceramics is rather low (approximately, 9.5 $\times$ 10^{-1} S/cm [10] the transport number of protons is higher than that of $BaCeO_3$-based ceramics.

Novick and Du [16], have reported a series of protonic conductors of the types $A_2(B'B'')O_3$ and $A_3(B'B'')O_9$ in which the A ions are always charged 2+ and $B'B''$ ions have 3+ and 5+ in the former system and 2+ and 5+ in the latter system. In all these systems, domains of different conductivity (ionic, electron, or hole conduction) can be observed, depending on the partial pressures of oxygen, water vapor, and temperature.

$SrCeO_3$ based ceramic electrolytes have been extensively investigated both electrically and structurally, due to the interest in their proton conducting properties [5]. However, little information exists on the effect of dopant concentration on each separate constituent of the total conductivity.

In ABO_3 perovskite type systems, when the A-site is substituted with an appropriate lower valency cation, oxygen vacancies are formed to maintain electroneutrality. Doping of the B-site in an ABO_3 perovskite with acceptor dopants is expected to increase the conductivity due to increased oxygen vacancies, protons and holes, but the full relevance and effects of this influence are not still clear.

The objective of this work was to study a $SrCeO_3$-based system, mainly stoichiometric $SrCe_{1-x}Y_xO_{3-\delta}$ (where x = 0.025, 0.05, 0.075, 0.1, 0.15, and 0.2, and $\delta = x/2$) and substoichiometric $Sr_{0.995}Ce_{0.95}Y_{0.05}O_{3-\delta}$, and resolve the total conductivity into its n-(electron), p-(hole), and i-(ionic) type conductivities. Each constituent was studied with regard to changing yttrium concentration and partial pressure of water.

2. Experimental

2.1. Synthesis of protonic conductive ceramics

The materials synthesized were stoichiometric $SrCeO_3$ based proton conductor perovskites consisting of $SrCe_{1-x}Y_xO_{3-\delta}$ (x = 0.025, 0.05, 0.075, 0.1, 0.15, and 0.2, and $\delta = x/2$) and substoichiometric $Sr_{0.995}Ce_{0.95}Y_{0.05}O_{3-\delta}$. The values of x were chosen to represent the range over which doping has the most effect on increasing the defect concentration (being 0–200%) of dopant without adversely affecting the overall stoichiometry, i.e., causing any second phase development by exceeding the upper limit of solid solution formation.

All samples were processed using a solid-state reaction. The reagents, $SrCO_3$, CeO_2, and Y_2O_3 were dried for 20 h at 150 °C and mixed in an agate ball mill. The calcination reactions were carried out in two steps, 1000 and 1300 °C with agate ball milling of 30 min and 1 h, respectively, between each calcination step. Dispersant (0.5 g PVP dissolved in 1 g ethanol per 100 g powder) was mixed into the powder, followed by 10 min of high speed ball milling and the samples were than formed into pellets of 10 mm diameter and approximately 2 mm thickness. Samples were then sintered at 1500 °C for 11 h. The surfaces of all the pellets were ground to a dull polished surface using SiC grinding papers with a grid of 1000 and 4000#. Pellets were then coated with platinum paste (Demetron Einbrennplatin 308A) and heated at 3 °C/min to 1125 °C for 2 h.

2.2. Evaluation of crystal structure and cell parameters

X-ray powder diffraction was performed at room temperature on a STOE theta–theta reflection diffractometer equipped with a Peltier cooled Kevex energy dispersive detector; Cu Kα radiation was used. The powdered samples were mixed with Si-standard. Unit cell dimensions were determined by the least squares method included in the Visual-X^{Pow} Stoe Software, which also allowed for adjustment of a zero-shift in 2-theta (were typically below 0.02°). X-ray diffraction data was used to confirm that the materials were single phase, and to allow calculation of the lattice constants of the materials.

2.3. Evaluation of theoretical density

Density measurements of the sintered samples were obtained using the standard Archimedes technique. In this method, the weight of a pelletized specimen is recorded before and after boiling in distilled water. The pellet is then suspended in water and re-weighed. The bulk density (B) is calculated using equation:

$$B = \frac{W_d}{W_w - W_s} \quad (1)$$

where W_d is the weight of dry sample; W_w the weight of wet sample; and W_s is the weight of sample suspended in water.

The theoretical density T_d was calculated from the equation:

$$T_d = \frac{ZM_C}{V_c N_A} \quad (2)$$

where Z is the number of chemical species in the unit cell; M_C the molar mass of a single chemical species corresponding to the chemical formula (g mol^{-1}); V_c the unit cell volume (UCV) (Å^3); N_A the Avogadro's number (6.0221 $\times$ 10^{23} mol^{-1}). The cell parameters were calculated using orthorhombic symmetry and $Z = 4$. Theoretical densities were estimated from XRD patterns using d spacing and a UNITCELL program parameter calculation. Unit cell dimensions

were determined by the least squares method included in the Visual-X^{pow} Stoe software, which allowed for adjustment of a zero-shift in 2-theta (typically below 0.02°). The percentage theoretical density (ρ%) was calculated using equation:

$$\rho = \frac{B}{T_d} \times 100\% \quad (3)$$

2.4. Evaluation of electrical conductivity

The electrical conductivity of the synthesized samples was determined as a function of oxygen partial pressure P_{O_2} at 400–800 °C range in two different atmospheres (P_{H_2O} = 0.01 and 0.001 atm) for each of the samples. A P_{O_2} range of 1 atm (pure O_2) to approximately, 1×10^{-25} atm (N_2/H_2 mix) allowed for the separation of n-(electron), p-(hole), and i-(ionic) type conductivities. A schematic of the overall P_{H_2O}/P_{O_2} testing apparatus is given in Fig. 1, where the dashed line represents the flow of gas through from the gas mixer to the sample and then out to the extraction system after testing.

The conductivity rig design, utilizes a pseudo four-point terminal system (a four wire, two electrode measurement system) to minimize the resistance due to wires, and could be run up to 1000 °C. The data presented, therefore, excluded the lead resistance, but included the electrode contact resistance. The computer program, FCL was used to control the overall experiment setup, as shown in Fig. 1. The computer accessed a multiplexer (3421A data acquisition/control unit by Hewlett Packard) containing a number of channels, which could access each piece of equipment separately. The system automated measurement readings from

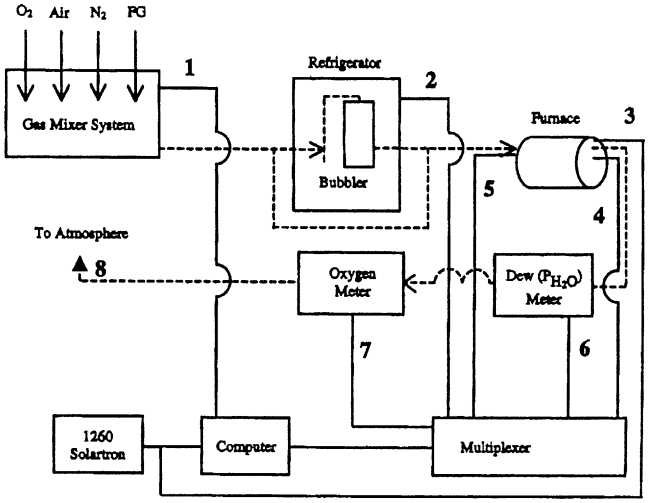

Fig. 1. Schematic of overall P_{H_2O}/P_{O_2} testing apparatus where, (1) computer control of mass flow controllers for automated gas mixing; (2) temperature thermocouple to refrigerator (constant 11 °C); (3) ac impedance cables connected to sample in furnace; (4) temperature thermocouple situated at sample in testing rig; (5) temperature thermocouple situated in furnace outside testing rig; (6) P_{H_2O} dew-point meter readings in percent atmospheres; (7) P_{O_2} readings in mV; (8) gas flow (total 100 mL/min) exhaust to extractor.

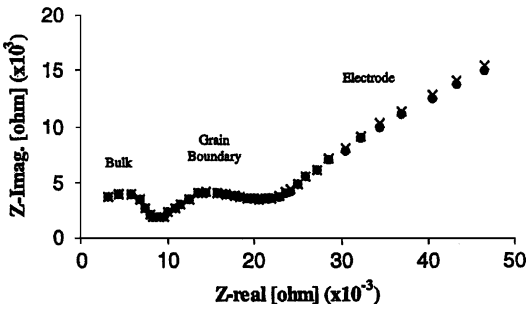

Fig. 2. Nyquist diagram showing real and fitted data for a $SrCeO_3$ based sample at 200 °C. (×) Fitted data, (●) actual data points, fit very close to actual).

P_{H_2O} meter, P_{O_2} meter, and of the control gas flow and overall control of the Solartron 1360 ac impedance/gain phase analyzer.

Brooks mass flow controllers (5850TR series) with a range of 100, 50, and 10 mL/min were computer controlled by the FCL program, thus, flow rates could be automatically monitored and changed throughout the experiment.

Conductivity measurements were undertaken in the frequency range 0.1 Hz to 1 MHz using Solartron 1360 impedance/gain phase analyzer.

When an ac impedance sweep is generated at lower temperatures, it is possible to resolve a curve, which represents bulk, grain boundary and electrode impedance as shown in Fig. 2. Using this data for each sample at two variables (temperature, P_{O_2}, P_{H_2O} = 0.01 atm) the corresponding conductivities were corrected for the relative density of each sample according to the linear relationship established in previous work [17]:

$$\sigma_r = \sigma_1[1 - 3(1 - d)] \quad (4)$$

where σ_1 is the conductivity of a 100% dense pellet and d is the ratio of measured to theoretical density. The latter was calculated from the formula molar mass, the number of formula in a unit cell and the unit cell volume as measured by X-ray diffraction. The conductivity at 100% density was determined by solving the equation for σ_1. Plots of log P_{O_2} versus conductivity were generated for each sample at each temperature and P_{H_2O} value. From these plots, a curve fit was generated that allowed for the resolution of p, n, and i values. The preliminary data obtained in this work show that resolution of the total conductivity down to its constituent elements allows studying the effect on conductivity with changing dopant concentration.

3. Results and discussion

3.1. Unit cell volume and density study of $SrCe_{1-x}Y_xO_{3-\delta}$ and substoichiometric $SrCe_{0.95}Y_{0.05}O_3$

The results of X-ray diffraction studies for powdered samples of $SrCe_{1-x}Y_xO_{3-\delta}$ (x = 0.025, 0.05, 0.075,

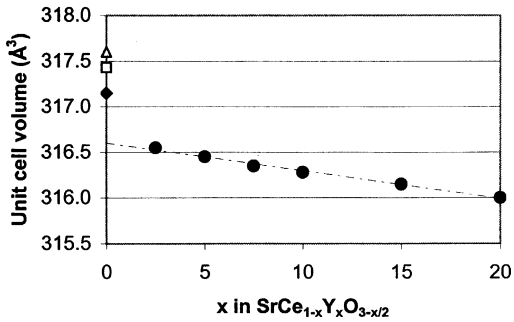

Fig. 3. Plot of unit cell volume(Å^3) vs. x in $SrCe_{1-x}Y_xO_{3-\delta}$. (●) This study, (◆) high-resolution neutron diffraction [20], (Δ) neutron diffraction [21], (□) powder XRD [23].

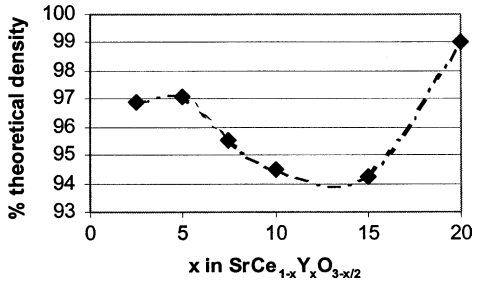

Fig. 4. Percentage of theoretical density vs. x in x in $SrCe_{1-x}Y_xO_{3-\delta}$.

0.1, 0.15, and 0.2, and $\delta = x/2$) and substoichiometric $Sr_{0.995}Ce_{0.95}Y_{0.05}O_{3-\delta}$ are given in Fig. 3. The calculated cell volume of undoped $SrCeO_3$ is compared to the data obtained previously by means of high-resolution neutron diffraction [18], neutron diffraction [19] and powder XRD [20].

The three unit cell volume determinations for undoped $SrCeO_3$ differ by almost 0.6 Å^3 which is above the experimental uncertainties of the high resolution X-ray and neutron diffraction measurements and can most likely be ascribed to slight deviations in A/B of the three systems.

The data presented in Fig. 3 shows a linear decrease of unit cell volume from $x = 0.025$ to 0.20. The effective ionic radius of Y^{3+} is 0.90 Å, which is larger, compared to 0.87 Å for Ce^{4+} cation. The fact that the lattice contracts when cerium is replaced by a slightly larger ion can only be interpreted as a result of tilting, or more efficient packing of the B–O octahedra, and/or relaxation of the ions around the oxygen vacancies introduced by doping. A similar study on $NaCe_{1-y}Nd_yO_{3-y/2}$ also showed a decrease in the unit cell volume from $y = 0$ to 0.12, although, in this case the mismatch between the radius of Nd^{3+} (0.983 Å) and Ce^{4+} is even larger.

The liner relationship, extrapolated to $x = 0$, is clearly 0.6–1.2 Å^3 below the three determinations for undoped $SrCeO_3$. Given that no change in space group occurs upon doping [19], the observed variation could be due to ordering of the Y_2O_3 dopant. It could also be due to substitution of a small amount of Y^{3+} on the A-site, accompanied by evolution of a small amount of Sr-rich phase. The ionic radius of Y^{3+} is available only for coordination of 5–9, not 12, observed for the perovskite A-site. Extrapolation from the available data indicates that the ionic radius of Y^{3+} in 12-fold coordination would be 1.25 Å, well below that of Sr (1.44 Å) in the same coordination. Thus, it may be inferred that substitution of Y_2O_3 on the A-site wilf reduce the unit cell volume. To clarify these effects, further studies are required at dopant levels below 2 mol%.

However, it should be noted that no cross-substitution effects have been revealed by careful neutron diffraction studies on several doped cerate systems [19].

In comparison to stoichiometric perovskites, the substoichiometric material studied, that of $Sr_{0.995}Ce_{0.95}Y_{0.05}O_3$, showed a drop in unit cell volume of approximately 0.34 Å^3 compared to its stoichiometric partner, $SrCe_{0.95}Y_{0.05}O_3$.

Theoretical density calculations using the X-ray data show a decrease in density with Y_2O_3 content (Fig. 4), which may be attributed to a distortion of the unit cell. The requirements for ceramic electrolytes are met at a low dopant concentration at $x = 0.02$ and 0.05, and at $x = 0.2$ where the relative density is in the range 97–99%. In the range from $x = 0.15$ to 0.075, the relative density is less than 95%, which does not meet the necessary requirements.

3.2. Electrical studies of proton conducting perovskites

The electrical conductivity in perovskite proton conducting oxides is known to be rather complicated combining both bonding and transport mechanisms. The proton has a small radius and thus, the isolated H ion is not present in solids under equilibrium conditions. Due to its strong polarizing power, H^+ is covalently bonded to one or two electronegative ions or atoms in the surrounding system. There are at least three different *bonding mechanisms* for the proton [21]:

1. The acceptor site for the proton may be an ion of the immobile lattice.
2. The proton may be attached to a mobile ion, for example, an oxygen ion forming OH^- (or $OH_0^\bullet$ using Kröger–Vink Notation).
3. The proton may be attached to a mobile molecule, such as H_2O.

Along with different bonding mechanisms, perovskite-based proton conductors support several *transport mechanisms* inducting both ionic and electronic. At low temperature, protonic 'hopping' between oxide ions is the dominant mechanism, whereas at high temperatures oxide ion migration usually results in p-type or less often in n-type conduction [22]. Another mechanism often applied to proton conduction is the 'vehicle' mechanism [17].

In earlier papers [5], the variation of conductivity with oxygen partial pressure for perovskite proton conductors has been described as:

$$\sigma_{tot} = \sigma_I + \sigma_n^0 {P_{O_2}}^{-1/4} + \sigma_p^0 {P_{O_2}}^{1/4} \quad (5)$$

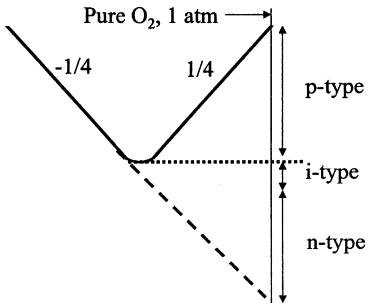

Fig. 5. Schematic where σ_i represents the P_{O_2}-invariant ionic (i-type) component and σ_n^0 and σ_p^0 represents the n- and p-type electronic components, respectively, extrapolated to an oxygen partial pressure of 1 atm.

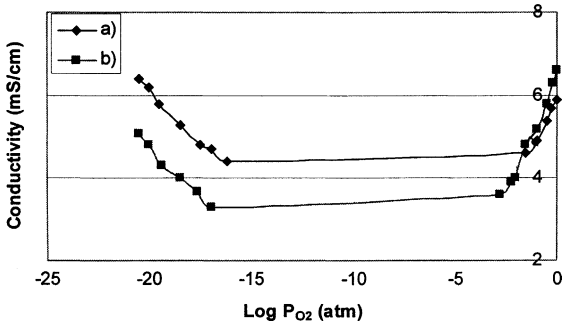

Fig. 6. Plot of electrical conductivity vs. P_{O_2} at $T = 800\,^{\circ}C$ and $P_{H_2O} = 0.01$ for $SrCe_{1-x}Y_xO_{3-\delta}$ (a) $SrCe_{0.9}Y_{0.1}O_{2.95}$; (b) $SrCe_{0.85}Y_{0.15}O_{2.95}$.

where σ_{tot} represents the total conductivity of the system, σ_i the P_{O_2} the invariant ionic component and σ_n^0 and σ_p^0, represent n- and p-type electronic components respectively, extrapolated to an oxygen partial pressure of 1 atm as illustrated in Fig. 5. Corresponding results for $Sr_{0.995}Ce_{0.95}Y_{0.05}O_{2.975}$ have been reported [19], which indicated the existence of an ionic conductivity component, independent of P_{O_2}, and two further components, designated p- and n-type electronic on the basis of their P_{O_2} dependencies. A similar conclusion was reached with Yb_2O_3-doped analogue [5]. However, according to Ahlgren [23], thermoelectric power studies of $SrCe_{0.95}Y_{0.05}O_{2.975}$ did not show any indication of n-type conductivity. Isotope studies of $Sr_{0.995}Ce_{0.95}Y_{0.05}O_{2.975}$ showed that the conductivity component appearing at low P_{O_2} displays an H/D isotope effect and, therefore, should be re-assigned to protonic.

Accordingly, in this work, the component appearing at low P_{O_2} has been provisionally been given the subscript "q" rather than "n".

3.2.1. Electrical studies of stoichiometric compounds $SrCe_{1-x}Y_xO_{3-\delta}$

Pure $SrCeO_3$ has low electronic conductivity in an oxygen atmosphere and does not behave as a proton conductor in a hydrogen-containing atmosphere [24]. Partial substitution by aliovalent cations such as Yb^{3+}, Sc^{3+}, and Y^{3+} for the Ce^{4+} site in the perovskite-type crystal $SrCeO_3$ play an important role in the appearance of proton conduction, however increasing the dopant cation concentration does not automatically cause an increase in total conductivity.

Typical plots of electrical conductivity in $SrCe_{1-x}Y_xO_{3-\delta}$ at $x = 0.15$ and 0.01 determined as a function of P_{O_2} at T=800 °C and $P_{H_2O} = 0.01$ atm in the range of $P_{O_2} = 1$ to 1×10^{-25} atm are shown in Fig. 6a and b. The solid lines on each figure represent fits to equation (1), in which the exponents in the P_{O_2} dependencies of p- and q-type conductivity were constrained to 1/4 and −1/4, respectively. The results give the conductivity contributions from each component. Inspection of equation (1) shows that parameters σ_p and σ_n have the physical meaning of the respective conductivities extrapolated to a partial pressure of 1 atm as shown by Fig. 5.The P_{O_2}-independent ionic component σ_i Fig. 7a and d, does not vary linearly with doping, as might be expected from a simple point defect description. Instead, it displays a maximum at $x = 0.10$, where it reaches 5 mS/cm. The occurrence of the maximum has been reported also for other cerate systems, for example, $BaCe_{1-x}Gd_xO_{3-\delta}$ [25]. The effect could be explained by the different level of saturation of water at different concentrations of dopant. The threshold effect has also been reported for the related system $SrCe_{1-x}Y_xO_{3-\delta}$ [26] at lower temperatures, where the conductivity is mainly protonic.

The p-type component, σ_p^0 Fig. 7b and e) shows the same threshold as the ionic component, but thereafter increases almost linearly with x. This is entirely consistent with the behavior of σ_i, since both the protonic carriers and the holes are generated from oxide ion vacancies according to rather similar equations. The absence of a maximum can be qualitatively explained by the fact that the holes are minority defects and their behavior deviates less from the predicted behavior than that of protons. In the other words, the oxygen dissolution equilibrium $1/4O_2\,(g) + 1/2Vo^{\bullet\bullet} \rightarrow 1/2O_0{}^x + h^{\bullet}$ is largely displaced to the left-hand side, making the hole concentration low, and therefore, less affected by dopant concentration. Comparing Fig. 8b with Fig. 8e, it can be seen that there is nearly a four times increase in each value. As the charge carriers in this oxide are protons and holes, the total conductivity σ_{total} is expressed as $\sigma_{total} = \sigma_H{}^{\bullet} + \sigma_h{}^{\bullet}$ where $\sigma_H{}^{\bullet}$ is the protonic component and $\sigma_h{}^{\bullet}$ is the p-type component or hole conduction. An increase in water vapor pressure would cause an increase in p-type conduction.

The component denoted by 'q' (Fig. 7c) at $P_{H_2O} = 0.01$, displays the opposite behavior to the p-type component, decreasing monotonically with doping level, indicating that it is related to the concentration of electrons. The decrease in P_{H_2O} from 0.01 to 0.001 atm (Fig. 7f) seems to have little effect on the q-type electronic conduction.

Returning to the apparent threshold effect in doping, two tentative explanations have been offered [27]. One is that at very low doping levels, the yttrium is concentrated at the grain boundaries and is, therefore, depleted in the bulk of the material; further addition of dopant produces the ex-

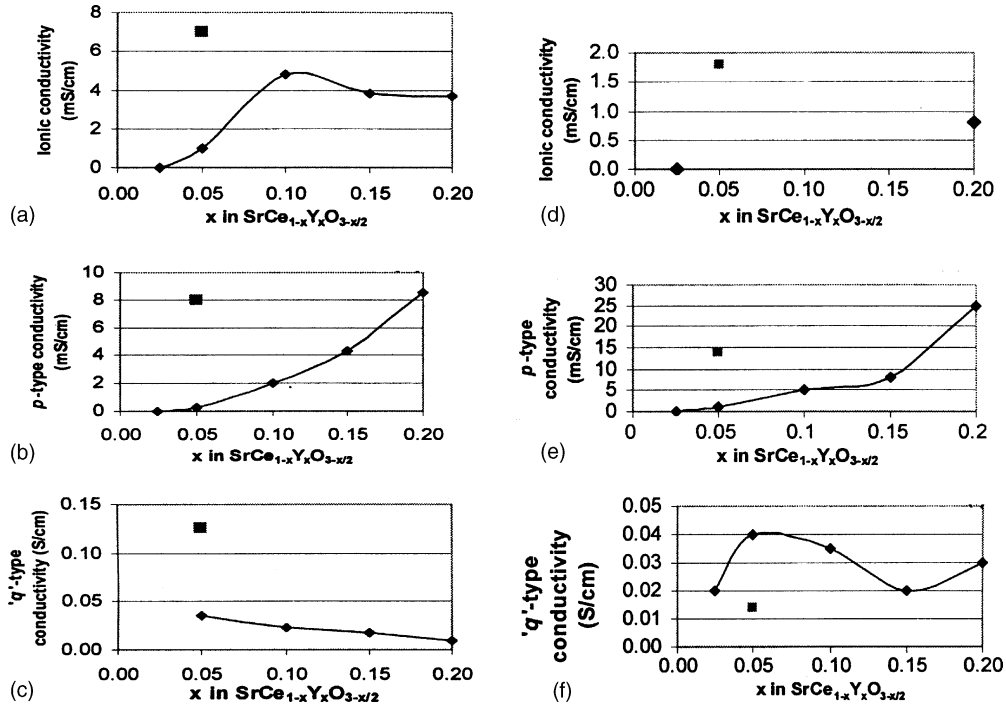

Fig. 7. Conductivity parameters, as determined for $SrCe_{1-x}Y_xO_{3-\delta}$ (◆) vs. at.% of yttrium dopant (x) for (a) ionic, (b) p-type, and (c) q-type conductivity at $T = 800\,^{\circ}C$ and $P_{H_2O} = 0.01$ atm, and (d) ionic, (e) p-type and (f) q-type conductivity at $T = 800\,^{\circ}C$ and $P_{H_2O} = 0.001$ atm where in each graph the square symbol (■) represents the substoichiometric material $Sr_{0.995}Ce_{0.95}Y_{0.05}O_{3-\delta}$.

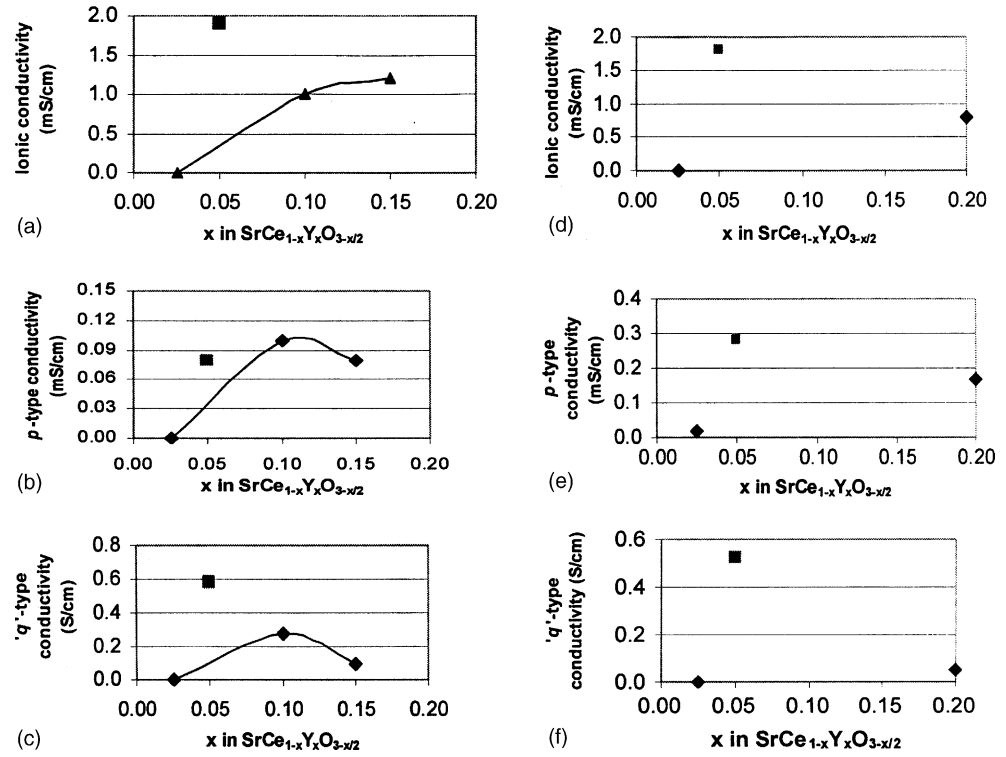

Fig. 8. Conductivity parameters, as determined for $SrCe_{1-x}Y_xO_{3-\delta}$ (◆) vs. at.% of yttrium dopant (x) for (a) ionic, (b) p-type, and (c) q-type conductivity at $T = 600\,^{\circ}C$ and $P_{H_2O} = 0.01$ atm, and (d) ionic, (e) p-type and (f) q-type conductivity at $T = 600\,^{\circ}C$ and $P_{H_2O} = 0.001$ atm where in each graph the square symbol (■) represents the substoichiometric material $Sr_{0.995}Ce_{0.95}Y_{0.05}O_{3-\delta}$.

pected increase in conductivity. An alternative explanation is partial substitution of Y_2O_3-dopant on A- and B-sites, which would generate no oxide ion vacancies and therefore no ionic conductivity.

The data presented in Fig. 7 does not give cause for preferring one or other explanation. On the other hand, a small degree of cross-substitution of Y^{3+} on the A-site would be qualitatively consistent with both the observed discontinuity of the unit cell volume, and the conductivity threshold for ionic and p-type components.

Electrical studies of $SrCe_{1-x}Y_xO_{3-\delta}$ for $P_{H_2O} = 0.01$ and 0.001 atm at $T = 600\,^{\circ}C$ (Fig. 8) show an expected drop in all conductivity values, due to higher impedance values at lower temperatures, and the trends. The trends shown at higher temperatures for each component appear to hold for the lower temperature at 600 °C.

3.2.2. Electrical studies of substoichiometric $Sr_{0.995}Ce_{0.95}Y_{0.05}0_{3-\delta}$

Figs. 7 and 8 show electrical conductivity data obtain for non-stoichiometric cerium based oxides at 800 and 600 °C, and two partial pressures of water vapor (0.01 and 0.001 atm). The square symbol represents the substoichiometric sample measurements for each component in each graph.

It can be seen that these values vary greatly from their stoichiometric partner, $SrCe_{0.95}Y_{0.05}O_3$. In all cases, the conductivity component is higher than that of the stoichiometric material, except for the q-type component at $P_{H_2O} = 0.001$ atm.

At 800 °C, the P_{O_2}-independent ionic component is 40% higher than its stoichiometric partner, being approximately 7 mS/cm for both partial pressures of water. The p-type component is also higher, nearly doubling from 8 to 14 mS/cm with decreasing P_{H_2O}.The q-type component shows a major decrease with decreasing P_{H_2O}.

At 600 °C (Fig. 8), ionic conductivity shows a similar trend as that observed for $T = 800\,^{\circ}C$, but with lower values. It has been speculated that the large deviations of each conductivity parameter caused by being substoichiometric on the A-site may be attributed to an increase in defect concentration. Sub-stoichiometry on the A site of an ABO_3 structure may introduce vacancies into the crystal structure, in the same way that doping with lower valence ion causes vacancies, however, more research is needed to confirm this assumption.

4. Conclusions

It has been shown, that changing the yttrium content in $SrCe_{1-x}Y_xO_{3-\delta}$ where $x = 0.025, 0.05, 0.075, 0.1, 0.15$, and 0.2 and $\delta = x/2$) affects the electrical and structural properties of the system. Unit cell volume and calculated density decrease with increasing yttrium content. In comparison to stoichiometric perovskites, the substoichiometric material studied, that of $Sr_{0.995}Ce_{0.95}Y_{0.05}O_3$, showed a drop in unit cell volume of approximately 0.34 $Å^3$ compared to its stoichiometric partner, $SrCe_{0.95}Y_{0.05}O_3$.

The ionic and p-type component of the conductivity show threshold effect with Y-doping, which may be related to the double substitution of Y on both A-and B-sites. A maximum ionic conductivity of 5 mS/cm was found at 10% Y, whereas p-type conductivity increases with increasing yttrium. A conductivity component appearing at low oxygen partial pressures decreases with yttrium doping. Substoichiometric $Sr_{0.995}Ce_{0.95}Y_{0.05}O_{3-\delta}$ has higher electrical conductivity than corresponding stoichiometric compound, being approximately, 7 mS/cm for both partial pressures of the water.

References

[1] W. Grover Coors, J. Power Sources 118 (2003) 150.
[2] T. Takahashi, H. Iwahara, Revue de Chim. Miner. 17 (1980) 243.
[3] H. Iwahara, T. Esaka, H. Uchida, N. Maeda, Solid State Ionics 3–4 (1981) 359.
[4] Y.S. Lin, Sep. Purif. Technol. 25 (2001) 39.
[5] I. Kosacki, H.L. Tuller, Solid State Ionics 80 (1995) 223.
[6] H. Iwahara, H. Uchida, N. Maeda, J. Power Sources 7 (1982) 7 193.
[7] T. Scherban, A.S. Nowick, Solid State Ionics 35 (1989) 189.
[8] N. Bonanos, B. Ellis, N.M. Mahmood, Solid State Ionics 44 (1991) 305.
[9] R.C.T. Slade, N. Smith, Solid State Ionics 61 (1993) 111.
[10] H. Iwahara, Solid State Ionics 86–88 (1996) 9.
[11] W. Lee, A.S. Nowick, L.A. Boaturner, Solid State Ionics 18–19 (1986) 989.
[12] T. Yajima, H. Kazeoka, T. Yogo, H. Iwahara, Solid State Ionics 47 (1991) 271.
[13] N. Tanigichi, K. Hatoh, J. Niikura, T. Gamo, H. Iwahara, Solid State Ionics 53–57 (1992) 998.
[14] H. Iwahara, T. Yajima, T. Hibino, H. Ushida, J. Electrochem. Soc. 140 (1993) 1687.
[15] K.D. Kreuger, E. Schonherr, J. Maier, Solid State Ionics 70–71 (1994) 278.
[16] A.S. Novick, Yang Du, Solid State Ionics 77 (1995) 137.
[17] E.O. Ahlgren, J.R. Hansen, N. Bonanos, F.W. Poulsen, Mogensen, in: Proceedings of the 17th International Symposium on Materials Science, 1996.
[18] K.S. Knight, N. Bonanos, Mater. Res. Bull 30 (1995) 347.
[19] J. Ranlov, B. Lebech, K. Nielsen, J. Mater. Chem. 5 (1995) 743.
[20] J. Ranlov, K. Nielsen, J. Mater. Chem. 4 (1994) 868.
[21] W. Gao, N.M. Sammes, An Introduction to Electronic, Ionic Materials, World Scientific Publishes, Singapore, 1999.
[22] U. Reichel, R.R. Arons, W. Schilling, Solid State Ionics 86–66 (1996) 639.
[23] E.O. Ahlgren, Solid States Ionics 97 (1997) 498.
[24] H. Uchida, N. Maeda, H. Iwahara, Solid State Ionics 11 (1983) 117.
[25] N. Bonanos, B. Ellis, K.S. Knight, N.M. Mahmood, Solid State Ionics 35 (1989) 179.
[26] H. Iwahara, H. Uchida, S. Tanaka, Solid State Ionics 9–10 (1983) 1021.
[27] J.F. Liu, A.S. Nowick, Solid State Ionics 50 (1992) 131.